STAINLESS STEEL REBAR FOR SEISMIC APPLICATIONS

Alberto Franchi[1], **Pietro Crespi**[1], **Aldo Bennani**[2] **and Marco Farinet**[2]
[1]*Politecnico di Milano, Milan, Italy*
E-mail: alberto.franchi@polimi.it, pietro.crespi@polimi.it
[2]*Cogne Acciai Speciali Aosta, Italy*
E-mail: aldo.bennani@cogne.com, marco.farinet@cogne.com

Abstract

This paper is meant to present the mechanical characteristics of austenitic stainless steel rebars under monotonic and cyclic loadings. Furthermore, some results concerning the experimental tests on column prototypes subjected to cyclic loadings are presented, with the intent of comparing with results obtained on analogous columns reinforced with standard high ductile carbon steel rebars.

Keywords: stainless steel, rebar, ductility, cyclic loading, seismic loading

1. Introduction

Stainless steel rebars are used primarily in reinforced concrete structures because of their corrosion resistance. It is well known from the literature (Park et al., 1982; Pipa and Carvalho, 1990; Monti and Nuti, 1992; Macchi et al., 1996; Franchi et al., 1996; Pantazopoulou, 1998; Riva and Franchi, 2001; Riva et al., 2001) that, for seismic applications, the reinforcing steel has to provide enough ductility, i.e. plastic elongation at ultimate stress, and enough strain hardening, measured by the ratio of ultimate stress over yield stress. At the same time, it is very well known from the literature, that austenitic stainless steel shows a remarkable degree of ductility and strain hardening. The question, therefore, comes out as follows: how does behave austenitic stainless steel reinforcement under seismic loading conditions?

2. Process Route

The melting shop used by Cogne Acciai Speciali (Aosta, Italy) for the production of standard stainless steel grades is equipped with an 80 Ton UHP furnace and an AOD converter with the same capacity (EC Report, 2005). The casting process carries out trough a continuous casting machine in square billet 160 mm. The billets are ground and inspected, in order to eliminate all the surface defects due to the casting operations. On line, the hot rolling process is performed in the wire rod and bar mill, consisting on a heating furnace, roughing stand and a continuous mill, capable of producing wire rod in coil from 5.5 to 32 mm and bars from 18 to 100 mm. The rolling mill provides to transform directly the billets into rebars, whose diameters can range between 14 to 50 mm; suitable heat treatment, sand blasting and picking process give the final surface aspect and mechanical characteristics to stainless steel rebars.

3. Tensile Tests under Monotonic Loading on AISI304 Ø16

Figure 2 shows the apparatus equipment for the quasi-static tensile tests under elongation control.

M. Pandey et al. (eds), Advances in Engineering Structures, Mechanics & Construction, 255–264.

Fig. 1. Rolling mill.

Fig 2. Elongation test apparatus.

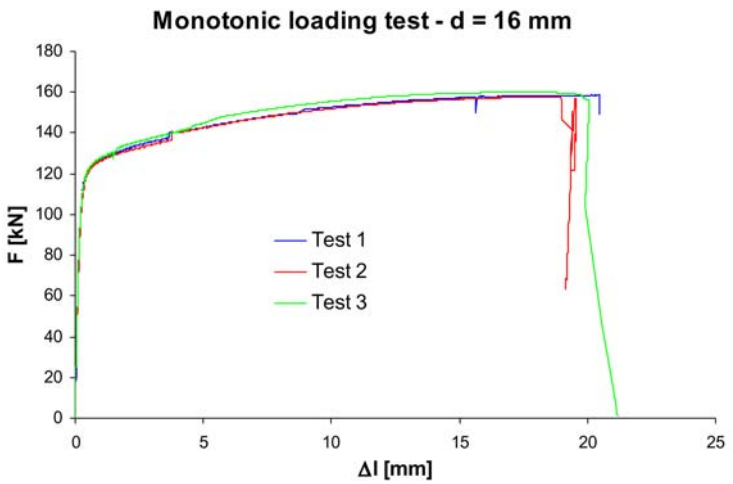

Fig. 3. Load-displacement of the tensile test.

The load-transducer displacement is reported for three analogous specimens in Figure 3. The end of the horizontal line of the graphs (about 20 mm) is due to the limited (20 mm) maximum elongation of the displacement transducer and not to the final stage of the stainless steel bar specimen.

3.1. *Results of the Monotonic Tensile Loading Test*

Figure 4 shows the stress-strain diagrams of the No. 3 stainless steel samples together with an optimized carbon "Tempcore" bar.

Experimental results concerning four major quantities, like yield stress-ultimate stress, ultimate over yield ratio, uniform elongation at maximum force are given in Table 1, in comparison with a 450 MPa carbon "Tempcore" steel rebar. It is evident that the AISI304 rebar is much superior with respect the carbon steel, even if this last is of the class 500 MPa instead of 450 MPa.

3.2. *Cyclic Loading on AISI304 Ø16 ($\Delta l/l = 1\%$)*

The geometrical data of the test specimen are given in Figure 5. The test has been repeated for three specimens. A mark every 10 mm has been placed along a straight line of the external surface in order to measure the uniform maximum elongation after failure (A_{gt}). The distance between the two grips

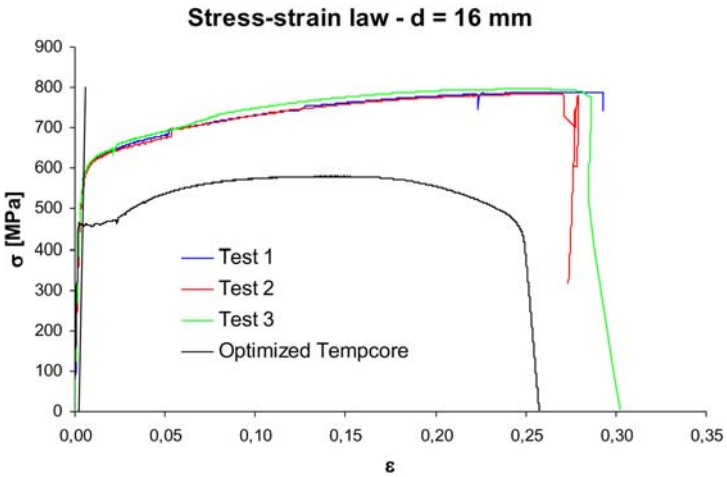

Fig. 4. Comparative results of the uniaxial tensile test between carbon and stainless steel rebar.

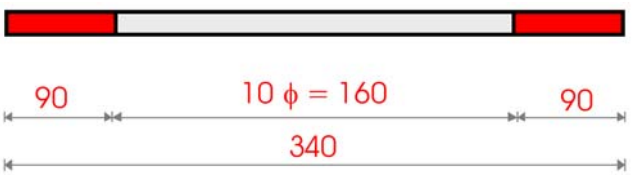

Fig. 5. Geometrical data of the specimens for the cyclic loading tests (dimensions in mm).

has been fixed to 10 times the diameter of the bar. The tests have been performed in displacement control with symmetric tension-compression cycles; frequency $1 \div 3$ Hz; amplitude of the imposed displacement: $\Delta L = \pm 1.6$ mm ($= 1\%$ of 160 mm).

3.3. *Results of the Cyclic Loading*

Figure 6 shows the hysteretic stress-strain diagram for about 200 cycles.

Figure 7 shows the load-displacement cyclic diagram but limited to the first 10 cycles; analogous cycles, corresponding to the carbon "Tempcore" rebar, are inserted, for comparison purposes, in the same figure.

It is interesting to point out: AISI304 presents higher values of the force for a given elongation than the carbon steel; this is because of the higher yield point and of the higher strain hardening of the AISI304 with respect the "Tempcore". The decrease of the maximum resistance, especially

Table 1. Resistances and ductility values.

	R_e [MPa]	R_m [MPa]	R_m/R_e	A_{gt} [%]
Inox (Ø16) test 1	558.01	788.89	1.41	29.00
Inox (Ø16) test 1	554.66	785.10	1.42	26.75
Tempcore (Ø14)	472.78	584.95	1.24	14.39
Tempcore (Ø14)	478.36	599.03	1.25	12.89

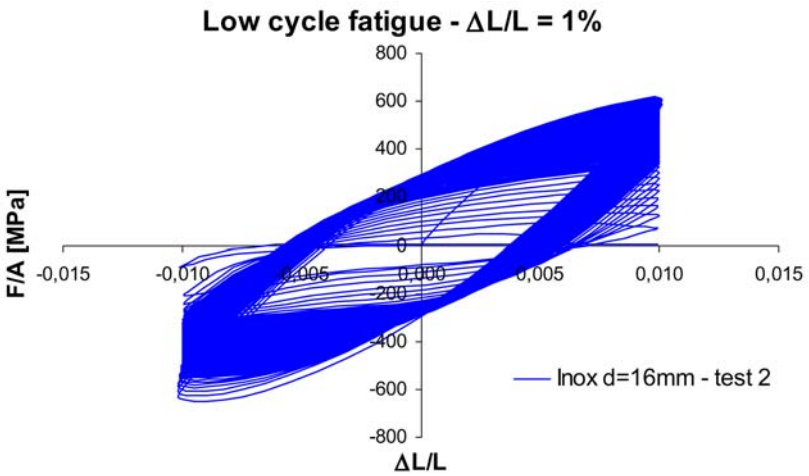

Fig. 6. Cyclic hysteretic load-displacement behaviour up to failure.

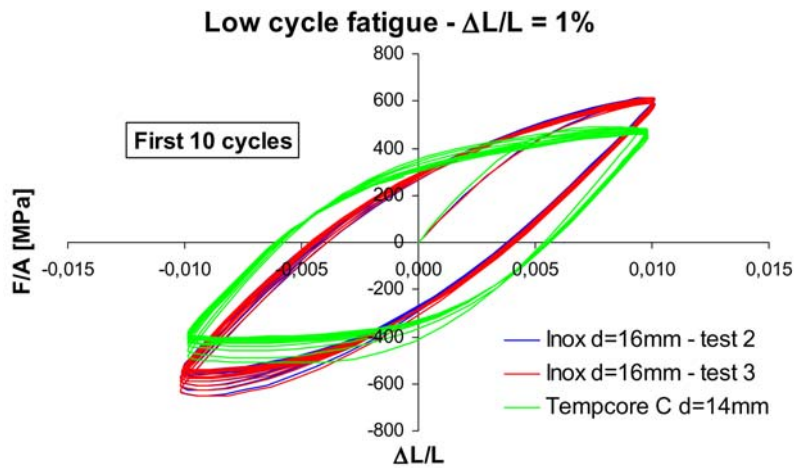

Fig. 7. Load-elongation hysteretic curves for the first 10 cycles.

in compression (i.e. in the negative side of the horizontal axis) is due to: (i) the crack initiation in the plastic hinge of the middle section and (ii) to the geometric effect, which is due to the fact that the pure compression mode becomes a bending-compression deformation mode. Figure 8 shows the decrease of the tension (greater values) and of the compression (smaller values) force along the cycles; it is evident how the carbon steel curve lies always below the lines of the AISI304. Low cycle fatigue resistance of AISI304 is almost twice (200÷250 cycles) as much as the carbon steel (100÷120 cycles).

Figure 9 gives total energy dissipation with the number of cycles, while Figure 10 gives the energy dissipated inside each cycle for all cycles.

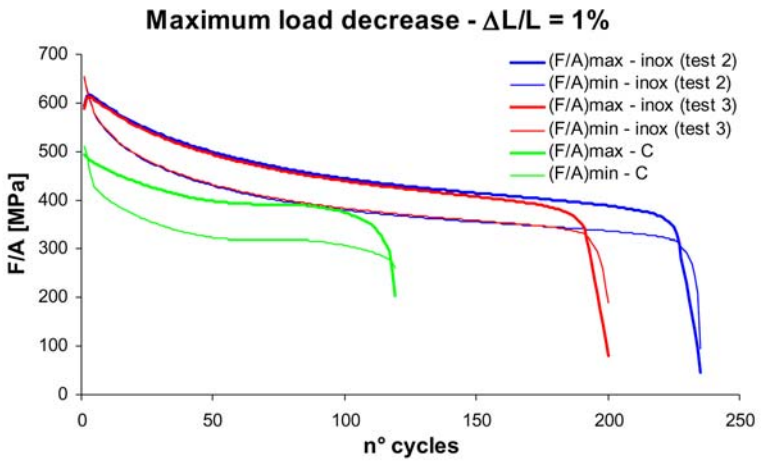

Fig. 8. Resistance decrease along the cycles.

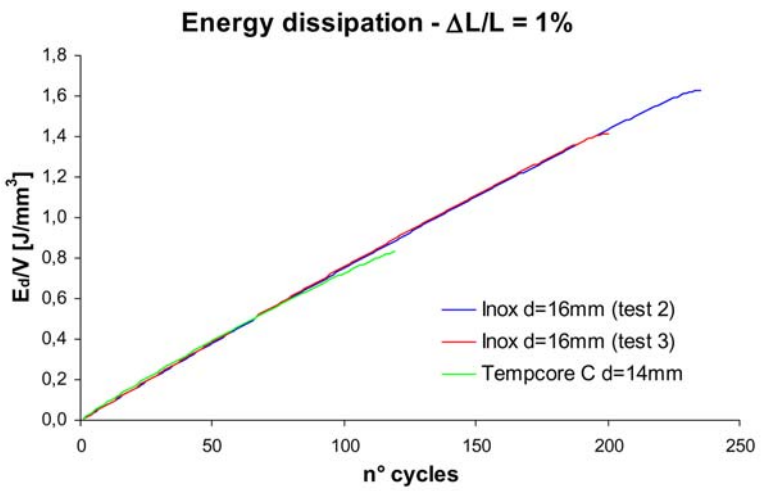

Fig. 9. Energy dissipation along the cycles.

4. Tests on R.C. Frames under Cyclic Loading

4.1. *The Prototype Design*

Figure 11 shows the steel reinforcement of the column and of the foundation. The steel reinforcement of the column consists of 4 Ø16 and stirrups Ø8 at 70 mm distance, inside the plastic hinge, made of AISI304.

4.2. *Test Rig*

The test apparatus consists of a stiff horizontal steel beam at which the foundation of the column is tight through two steel plates connected by 4 pre-tensioned steel bars. The r.c. foundation has been designed in such a way that it remains in the elastic domain while the plastic hinge will develop at the bottom part of the column. The top section of the column is connected to a horizontal actuator

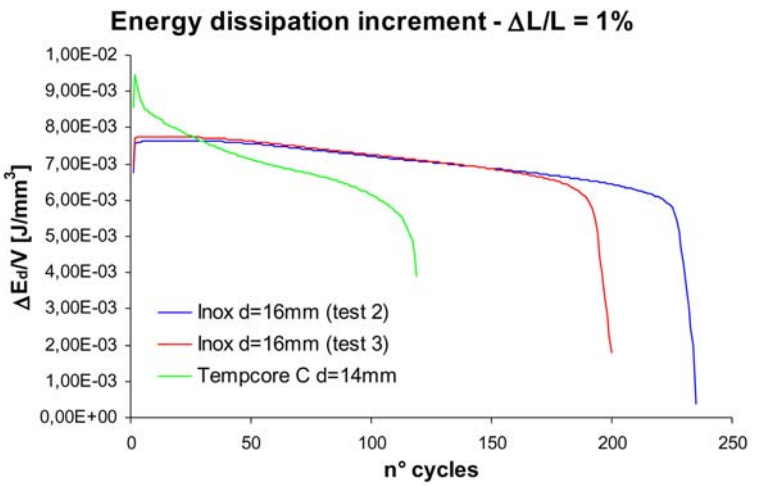

Fig. 10. Variation of energy dissipation in any cycle.

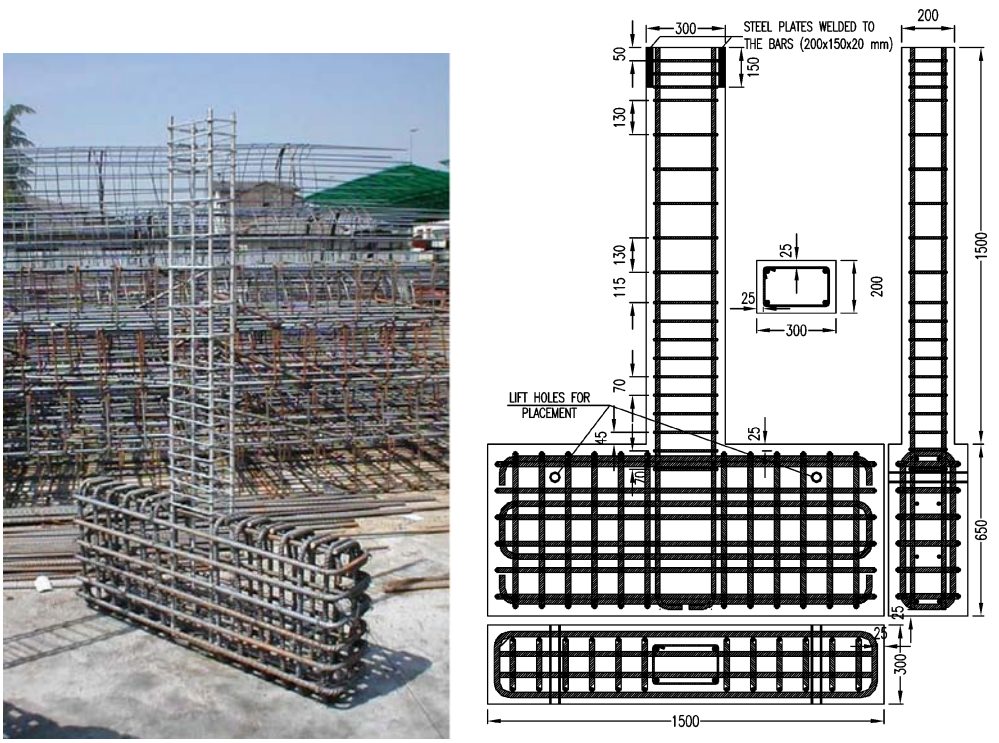

Fig. 11. Steel reinforcement of the column prototype.

Fig. 12. Test rig and the column prototype.

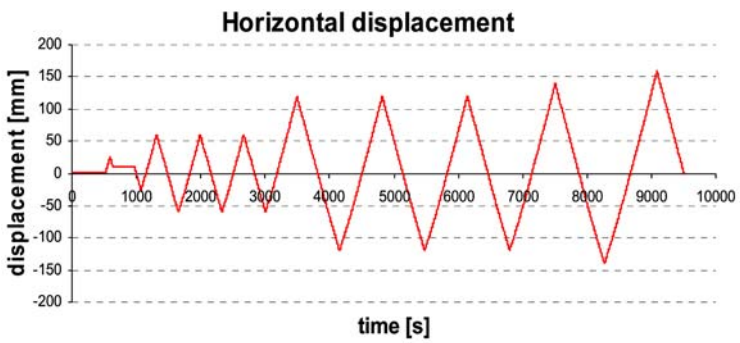

Fig. 13. Horizontal displacement of the top section of the column.

in displacement control. It moves cyclically, to the left and to the right with respect to the initial configuration, of a given horizontal displacement. The horizontal actuator is connected to a load cell, which gives the horizontal applied force, and a horizontal displacement transducer gives the horizontal displacement. Figure 12 shows also the vertical displacement transducers, located in the bottom of the column, which are necessary for evaluating the "plastic hinge" rotation.

4.3. *Loading History*

The tests are performed under displacement control, i.e. the horizontal displacement of the top of the column is imposed by the electro-mechanical displacement actuator and the corresponding horizontal force is measured by the load cell. The displacement time history is illustrated in Figure 13.

A first cycle is performed in order to evaluate δ_y, i.e. that displacement at which, for the first time, yield is reached in a point of the steel reinforcement. Then three cycles are performed by reaching $\pm 3\delta_y$ and another three cycles attaining $\pm 6\delta_y$. If the steel does not break, the steel could be defined as a high ductility steel reinforcement.

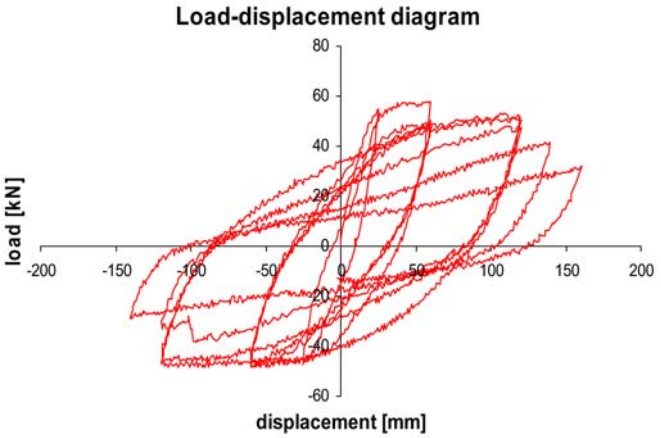

Fig. 14. Load-displacement curves of the top section of the column.

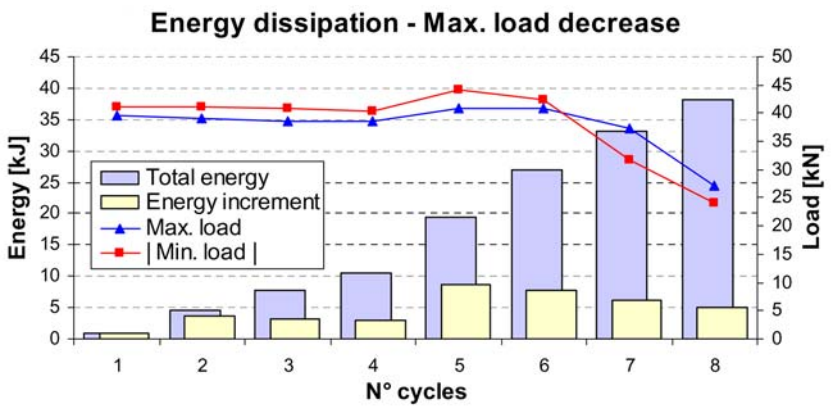

Fig. 15. Carbon steel energy dissipation.

4.4. *Results*

Figure 14 shows a load-displacement hysteretic cyclic diagram. It shows a decrease of the peak load during the cycles, mainly due to both a damage of the steel reinforcement and geometrical effects, i.e. the instability of compressed bars which deform in a flexural mode instead of a pure axial mode. The slope of the curves is a measure of the stiffness of the column and it presents two different situations: (i) an elastic phase, i.e. a phase where the steel bars load or unload in the elastic regime; (ii) an elastic plastic stage, where the bars are loaded in tension or in compression/bending in the plastic range; these slopes are continuously decreasing because of the continuous damage of the concrete material during the cycles.

The bar chart of Figures 15 and 16 shows, for each cycle, the maximum horizontal force and the cumulative dissipated energy, expressed as a function of the cycle number.

It is easy to verify that the maximum load carried out by the column reinforced by stainless steel is more than 20% the corresponding reinforced with carbon steel and, more important, the resistance stays constant during the cycles more than the columns reinforced with “carbon” steel. The total energy dissipated is almost twice in favour of the stainless steel.

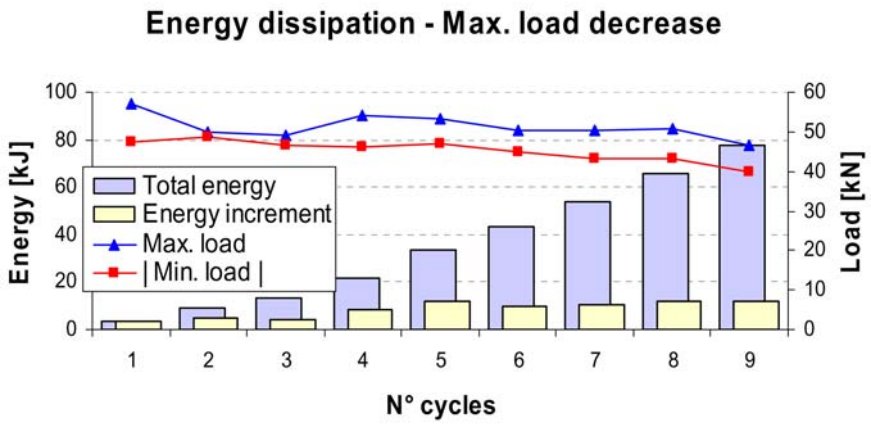

Fig. 16. Stainless steel energy dissipation.

Fig. 17. Details of the plastic hinge at the final stage.

We can conclude that the same column, reinforced with stainless steel, will present after the same seismic action, probably, very less severe damages than the analogous column reinforced with carbon steel. Figure 17 shows pictures of the damaged "plastic hinge" at the final cycle of the loading history. It may be interesting to remark that some specimen present a plastic tube which prevent bond between the longitudinal bar and the concrete in the plastic hinge zone. The question was: does the bond influence the behaviour of the plastic hinge? The answer is: no. Interesting to observe in the right picture on the top of Figure 17 that the deformation of the "plastic hinge" is mainly due to shear; this happens when the concrete trust has collapsed. If the steel bar does not fail, then shear may be considered as the collapse mode of the column. The stainless steel greater strain hardening behaviour imposes a revision, in Eurocodes 2 and 8 (EN1992, 2004, EN1998, 2004), of the maximum shear

force the reinforced concrete member has to sustain if maximum advantage of the stainless steel resistance has to be exploit. Otherwise, like shown in the left picture of the second row, a failure of a stirrup is very likely to happen.

5. Conclusions

AISI304 stainless steel rebars have been tested under quasi-static tensile load as well as under tension-compression cyclic loading. The class of resistance is a 500 MPa characteristic yield limit. The rebars have demonstrated unusual ductility level, both in the monotonic and the cyclic loading, as compared to traditional carbon steel rebars. Tests on column prototypes have shown an analogous ductile structural behaviour but at a higher horizontal force. This fact suggests the idea of using stainless steel in seismic areas for a more limited behaviour factor (larger horizontal forces) but using, at the same time, a limited steel area (because of the higher resistance of the stainless steel) and therefore resulting in expected limited damages to the structure after the earthquake.

Acknowledgement

The technical and financial support of Cogne Acciai Speciali of Aosta, Italy, is gratefully acknowledged.

References

EC, 2005, HIPER – Increase Infrastructure Reliability by Developing a Low Cost and High Performance Stainless Steel Rebar, Growth Programma, Final Report, 2005-12-09.

EC, SRD, Technical Steel Research, "Optimization of Ductility of Welded Steel Bars, Ribbed Coils and Mesh Fabric for Reinforced Concrete Elements under Severe Seismic Loads, Report EUR20506 EN.

EN1992-1-1, 2004, Eurocode 2: Design of Concrete Structures – Part 1: General Rules and Rules for Buildings.

EN1998, 2004, Eurocode 8: Design of Structures for Earthquake Resistance.

Franchi, A., Riva, P., Ronca, P., Roberti, R. and La Vecchia M., 1996, Failure Modalities of Reinforcement Bars in Reinforcing Concrete Elements under Cyclic Loading, *Studi e Ricerche*, Vol. 17, 157–187.

Macchi, G., Pinto, P. and Sanpaolesi, L., 1996, Ductility Requirements for Reinforcement under Eurocodes, *Structural Engineering International*, Vol. 4, 249–254.

Monti, G. and Nuti, C., 1992, Nonlinear Cyclic Behaviour of Reinforcing Bars Including Buckling, *Journal of Structural Engineering*, Vol. 118(12), 3268–3284.

Pantazopoulou, S.J., 1998, Detailing for Reinforcement Stability in R.C. Members, *ASCE Journal of Structural Engineering*, Vol. 124(6), June, 623–632.

Park, R., Priesley, M.J.N. and Gill, W.D., 1982, Ductility of Square Confined Concrete Columns, *Journal of the Structural Division, ASCE*, Vol. 108 (No. ST4), April, 929–950.

Pipa, M. and Carvalho, E.C., 1990, Experimental Evaluation of the Behaviour of Structures Designed for Two Ductility Levels, *European Earthquake Engineering*, Vol. 4(1).

Riva, P. and Franchi, A., 2001, Behaviour of Reinforced Concrete Walls with Welded Wire Mesh Subjected to Cyclic Loading, *ACI Struct. Journal*, May–June, 324–334.

Riva, P, Franchi, A. and Tabeni D., 2001, Welded Tempcore Reinforcement Behaviour for Seismic Applications, *Materials and Structures*, Vol. 34, May, 240–247.